

Article

Pairwise Coded *m*CAP with Chaotic Dual-Mode Index Modulation for Secure Bandlimited VLC Systems

Yungui Nie ^{1,†}, Wei Zhang ^{2,†}, Yanbing Yang ³, Xiong Deng ⁴, Min Liu ¹ and Chen Chen ^{1,*} 

¹ School of Microelectronics and Communication Engineering, Chongqing University, Chongqing 400044, China; 202012021020t@cqu.edu.cn (Y.N.); liumin@cqu.edu.cn (M.L.)

² Institute of Cyberspace Security, China Electronic Technology Cyber Security Co., Ltd., Chengdu 610041, China; zhangw9761@cetcs.com

³ College of Computer Science, Sichuan University, Chengdu 610065, China; yangyanbing@scu.edu.cn

⁴ Center for Information Photonics and Communications, School of Information Science and Technology, Southwest Jiaotong University, Chengdu 611756, China; xiongdeng@swjtu.edu.cn

* Correspondence: c.chen@cqu.edu.cn

† These authors contributed equally to this work.

Abstract: In this paper, for the first time, we propose and experimentally demonstrate a novel pairwise coding (PWC)-based multiband carrierless amplitude and phase (*m*CAP) modulation with chaotic dual-mode index modulation (DM) for secure bandlimited visible light communication (VLC) systems. The combination of *m*CAP and DM can sustain a higher spectral efficiency (SE) compared with *m*CAP with conventional index modulation (IM), while PWC can be employed to efficiently mitigate the signal-to-noise ratio (SNR) imbalance caused by the low-pass frequency response of light emitting diodes (LEDs). Moreover, the DM is enhanced by a two-dimensional (2D) chaotic encryption scheme to guarantee the security of the useful information in VLC systems. Simulation and experimental results successfully verify the superiority of the proposed PWC-based *m*CAP-DM scheme with two-level chaotic encryption over other benchmark schemes.

Keywords: visible light communication (VLC); carrierless amplitude and phase (CAP) modulation; pairwise coding (PWC); dual-mode index modulation (DM); chaotic encryption



Citation: Nie, Y.; Zhang, W.; Yang, Y.; Deng, X.; Liu, M.; Chen, C. Pairwise Coded *m*CAP with Chaotic Dual-Mode Index Modulation for Secure Bandlimited VLC Systems. *Photonics* **2022**, *9*, 141. <https://doi.org/10.3390/photonics9030141>

Received: 12 February 2022

Accepted: 25 February 2022

Published: 27 February 2022

Publisher's Note: MDPI stays neutral with regard to jurisdictional claims in published maps and institutional affiliations.



Copyright: © 2022 by the authors. Licensee MDPI, Basel, Switzerland. This article is an open access article distributed under the terms and conditions of the Creative Commons Attribution (CC BY) license (<https://creativecommons.org/licenses/by/4.0/>).

1. Introduction

Visible light communication (VLC) utilizing commercially available light emitting diodes (LEDs) has become more appealing to the sixth generation (6G) and Internet of Things (IoT) systems, due to its enormous merits of abundant and unregulated spectrum resources, no electromagnetic radiation and high security [1,2]. However, the achievable capacity of practical VLC systems is greatly restrained by the small modulation bandwidth and the severe nonlinearity of off-the-shelf LEDs [3].

Many techniques have been proposed to expand the available bandwidth for VLC systems. For one thing, analog or digital equalization techniques can be applied to break the limited bandwidth of LEDs [4,5]. For another thing, various spectrally efficient modulation and multiple access techniques, including carrierless amplitude and phase (CAP) modulation, orthogonal frequency division multiplexing (OFDM) with high-order modulation formats, multiple-input multiple-output (MIMO) and nonorthogonal multiple access (NOMA), can also be considered to enhance the achievable data rate of VLC systems [6–9]. Moreover, CAP has the benefits of a lower implementation cost and lower peak-to-average power ratio (PAPR) in comparison to OFDM. To increase the link performance, multiband CAP (*m*CAP) has been further proposed, which splits the available signal bandwidth into *m* subbands so as to improve the tolerance against the low-pass effect of LEDs [10].

Recently, a novel *m*CAP with index modulation (*m*CAP-IM) technique has been proposed to obtain better bit error rate (BER) performance than classical *m*CAP. In *m*CAP-IM,

the subbands of classical *mCAP* are divided into two parts: the active and inactive subbands. The active subbands can be modulated by constellation data symbols while the inactive subbands are nulled [11]. To further enhance the spectral efficiency (SE) of *mCAP-IM*, *mCAP* with dual-mode index modulation (*mCAP-DM*) has been proposed in [12], where all subbands are modulated to transmit data symbols. Moreover, the detection of signals plays an important role in optical wireless communication systems. In [13], a novel high-dimensional (HD) noncoherent detection scheme was proposed for multi-intensity-modulated ultraviolet communication (UVC) systems to address the intersymbol interference (ISI) issue. In [14], a sparse signal detection scheme exploiting the sparse reconstruction algorithms in compressed sensing (CS) was proposed for indoor VLC systems using generalized space shift keying (GSSK). For VLC systems employing *mCAP-DM*, the low-complexity near-optimal log-likelihood rate (LLR) detector is generally adopted [11,12]. For practical *mCAP-DM* VLC systems, the signal-to-noise ratio (SNR) of high-frequency subbands imposes inevitable degradation compared with that of low-frequency subbands. Hence, all subbands are in the condition of unbalanced SNR, which results in the degradation of the overall BER performance. In order to resolve the issue of unbalanced SNR, pairwise coding (PWC) can be introduced to improve the overall system performance, which requires no overhead and exhibits low computation complexity [15]. Although VLC has inherent security against eavesdroppers outside its coverage, the confidential information might still be eavesdropped by unintended or unauthorized users when they are located within the system coverage [16].

In this paper, we propose and investigate a novel PWC-based *mCAP-DM* scheme with two-dimensional (2D) chaotic encryption for practical VLC systems. The superiority of the proposed *mCAP-DM* scheme was successfully verified by both numerical simulations and hardware experiments.

2. PWC-Based *mCAP-DM* with 2D Chaotic Encryption

2.1. Principle

Figure 1a,b illustrate the block diagrams of the transmitter and receiver of the proposed PWC-based *mCAP-DM* with 2D chaotic encryption, respectively. In the transmitter, the input bits are firstly divided into G groups through a bit splitter and every group of b bits is used to generate an *mCAP* subblock of length N . Subsequently, every b bits is further partitioned into the index bits b_i and the constellation bits b_c , i.e., $b = b_i + b_c$. More specifically, the b_i bits are used to select the indices of k subbands out of N subbands in total via a chaotic index selector, while the b_c bits are employed to generate the corresponding constellation symbols to perform DM through a chaotic constellation mapper. Assuming the selected k subbands adopt constellation mode 1 while the remaining $N - k$ subbands adopt constellation mode 2, the two constellation sets corresponding to constellation modes 1 and 2 can be denoted by $\mathcal{M}_1 = [S_1^1, S_2^1, \dots, S_{M_1}^1]^T$ with size M_1 and $\mathcal{M}_2 = [S_1^2, S_2^2, \dots, S_{M_2}^2]^T$ with size M_2 , respectively, where $(\cdot)^T$ denotes the transpose operation. Since \mathcal{M}_1 and \mathcal{M}_2 are two distinguishable constellation sets, we have $\mathcal{M}_1 \cap \mathcal{M}_2 = \emptyset$. The detailed principle of DM with 2D chaotic encryption is introduced in the following subsection. Subsequently, the *mCAP* block can be created by concatenating G subblocks through a block creator. Before executing upsampling, PWC encoding is performed to mitigate the SNR imbalance. After passing through the in-phase (I) and quadrature (Q) filters, the transmitted PWC-based *mCAP-DM* signal with 2D chaotic encryption is obtained. Specifically, the impulse responses of a pair of orthogonal I and Q filters for the n -th ($n = 1, \dots, m$) subband can be, respectively, expressed as

$$f_n^I(t) = g(t)\cos(2\pi f_{c,n}t), \tag{1}$$

$$f_n^Q(t) = g(t)\sin(2\pi f_{c,n}t), \tag{2}$$

where $g(t)$ is the impulse response of the baseband shaping filter and $f_{c,n}$ denotes the center frequency of n th subband. The root raised cosine filter (RRCF) was adopted as the baseband shaping filter in this work [10].

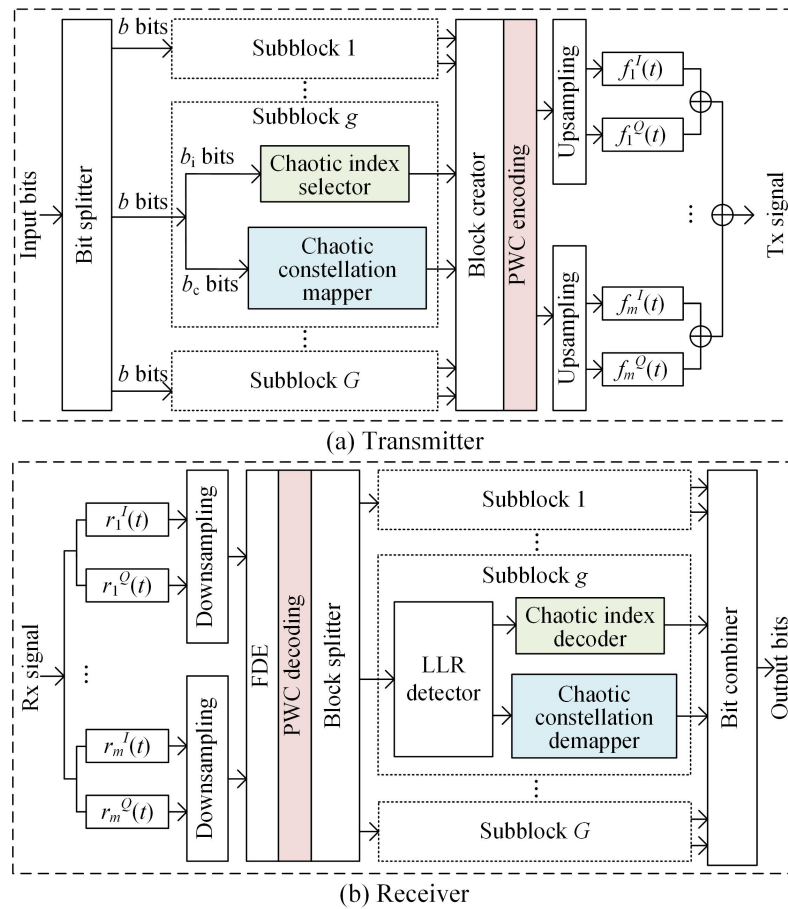


Figure 1. Block diagrams of the proposed PWC-based *mCAP-DM* with 2D chaotic encryption: (a) transmitter and (b) receiver.

In the receiver, as shown in Figure 1b, the received signal first passes through *m* pairs of matched filters and the impulse responses of the matched filters for the *n*th subband are given by

$$r_n^I(t) = f_n^I(-t), \tag{3}$$

$$r_n^Q(t) = f_n^Q(-t). \tag{4}$$

After downsampling, frequency-domain equalization (FDE) and PWC decoding are performed to recover the data symbols on each subband. Subsequently, the *mCAP* block is divided into *G* subblocks by a block splitter. The signal of each subblock can be detected by a low-complexity LLR detector. Letting y_g^η ($g = 1, \dots, G; \eta = 1, \dots, N$) be the input signal, the corresponding LLR value for the *g*th subblock is given by

$$\lambda_g^\eta = C + \ln \left(\sum_{i=1}^{M_1} \exp \left(-\frac{|y_g^\eta - S_i^1|^2}{N_0} \right) \right) - \ln \left(\sum_{j=1}^{M_2} \exp \left(-\frac{|y_g^\eta - S_j^2|^2}{N_0} \right) \right), \tag{5}$$

where $C = \ln(k) - \ln(N - k)$ and N_0 denotes the noise power. After subblock detection in each subblock, the index bits and the constellation bits can be recovered via a chaotic index decoder and a chaotic constellation demapper, respectively. Finally, the obtained index bits and constellation bits are combined by a bit combiner to yield the output bits.

As a result, the SE of the *mCAP-DM* signal is calculated by

$$SE_{mCAP-DM} = \frac{b_i + b_c}{N} = \frac{\lfloor \log_2(C(N, k)) \rfloor + k \log_2(M_1) + (N - k) \log_2(M_2)}{N}, \tag{6}$$

where $\lfloor \cdot \rfloor$ represents the floor operator and $C(\cdot, \cdot)$ denotes the binomial coefficient. It should be noted that the SE of the m CAP-DM signal is not affected by the PWC coding and 2D chaotic encryption. In contrast, since only the selected subbands are used to modulate constellation symbols while the remaining subbands are left unmodulated in m CAP-IM, the SE of m CAP-IM is expressed by

$$SE_{m\text{CAP-IM}} = \frac{\lfloor \log_2(C(N, k)) \rfloor + k \log_2(M)}{N}, \tag{7}$$

where M is the size of the constellation modulated on the selected subbands in m CAP-IM.

2.2. DM with 2D Chaotic Encryption

The principle of DM with 2D chaotic encryption is described as follows. As can be seen from Figure 1a, the proposed 2D chaotic encryption scheme is performed with respect to each m CAP subblock, which mainly consists of the following two chaotic scrambling processes: one is the chaotic constellation scrambling (CCS) and the other is the chaotic mode scrambling (CMS). In each subblock, CCS and CMS are performed via the chaotic constellation mapper and the chaotic index selector, respectively.

For the m CAP-DM system with two distinguishable constellation sets, i.e., \mathcal{M}_1 and \mathcal{M}_2 , the CCS process is conducted with respect to each constellation set. Letting $\mathbf{p}_g^1 = [p_{g,1}^1, p_{g,2}^1, \dots, p_{g,M_1}^1]^T$ and $\mathbf{p}_g^2 = [p_{g,1}^2, p_{g,2}^2, \dots, p_{g,M_2}^2]^T$ denote, respectively, the corresponding permutation vectors for \mathcal{M}_1 and \mathcal{M}_2 in the g th subblock with $g = 1, \dots, G$, the resultant constellation sets corresponding to \mathcal{M}_1 and \mathcal{M}_2 after performing CCS are expressed as follows:

$$\mathcal{M}_1^{\text{CCS}} = \text{src}\{\mathcal{M}_1, \mathbf{p}_g^1\} = [S_{p_{g,1}^1}^1, S_{p_{g,2}^1}^1, \dots, S_{p_{g,M_1}^1}^1]^T, \tag{8}$$

$$\mathcal{M}_2^{\text{CCS}} = \text{src}\{\mathcal{M}_2, \mathbf{p}_g^2\} = [S_{p_{g,1}^2}^2, S_{p_{g,2}^2}^2, \dots, S_{p_{g,M_2}^2}^2]^T, \tag{9}$$

where $\text{src}\{\cdot, \cdot\}$ denotes the scrambling function that scrambles \mathcal{M}_1 and \mathcal{M}_2 according to their respective permutation vectors \mathbf{p}_g^1 and \mathbf{p}_g^2 , where the permutation vector contains the new positions of the constellation points in the corresponding constellation set.

Moreover, the CMS process is performed with respect to the two constellation modes during the DM within each subblock. In the DM without applying CMS, each constellation mode corresponds to a fixed constellation set. However, in the CMS-encrypted DM, the corresponding relationship between two constellation modes, i.e., mode 1 and mode 2, and two encrypted constellation sets $\mathcal{M}_1^{\text{CCS}}$ and $\mathcal{M}_2^{\text{CCS}}$ is scrambled according to a binary scrambling vector. Letting $\mathbf{s} = [s_1, s_2, \dots, s_G]^T$ denote the binary scrambling vector for the m CAP block with a total of G subblocks, the corresponding relationship between two constellation modes and two encrypted constellation sets in the g th ($g = 1, \dots, G$) subblock is given in Table 1. As we can see, when $s_g = 0$, the two encrypted constellation sets corresponding to mode 1 and mode 2 are $\mathcal{M}_1^{\text{CCS}}$ and $\mathcal{M}_2^{\text{CCS}}$, respectively. However, when $s_g = 1$, the corresponding relationship becomes reversed, i.e., the two encrypted constellation sets corresponding to mode 1 and mode 2 become $\mathcal{M}_2^{\text{CCS}}$ and $\mathcal{M}_1^{\text{CCS}}$, respectively.

Table 1. Corresponding relationship of CMS in the g th subblock.

	$s_g = 0$	$s_g = 1$
Mode 1	$\mathcal{M}_1^{\text{CCS}}$	$\mathcal{M}_2^{\text{CCS}}$
Mode 2	$\mathcal{M}_2^{\text{CCS}}$	$\mathcal{M}_1^{\text{CCS}}$

By performing DM with 2D chaotic encryption, including CCS and CMS, the physical-layer security of m CAP-DM can be greatly enhanced. In order to successfully perform CCS and CMS, the permutation vectors \mathbf{p}_g^1 and \mathbf{p}_g^2 with respect to the g th subblock and the binary scrambling vector \mathbf{s} with respect to the m CAP block with a total of G subblocks

should be obtained in advance. In this work, the Hitzl–Zelev chaotic map is adopted to simultaneously generate the permutation vectors \mathbf{p}_g^1 and \mathbf{p}_g^2 and the binary scrambling vector \mathbf{s} , which is expressed by [17]

$$\begin{cases} x_{q+1} = 1 + y_q - z_q x_q^2 \\ y_{q+1} = \alpha x_q \\ z_{q+1} = \beta x_q^2 + z_q - 0.5 \end{cases}, \tag{10}$$

where α and β are the bifurcation parameters. When $\alpha = 0.25$ and $\beta = 0.87$, the Hitzl–Zelev chaotic map exhibits chaotic behavior. Based on the Hitzl–Zelev chaotic map, the permutation vectors \mathbf{p}_g^1 and \mathbf{p}_g^2 can be generated by using the states x_q and y_q as follows:

$$\mathbf{p}_g^1 = \text{sort}\{[x_{K+1}, x_{K+2}, \dots, x_{K+M_1}]^T\}, \tag{11}$$

$$\mathbf{p}_g^2 = \text{sort}\{[y_{K+1}, y_{K+2}, \dots, y_{K+M_2}]^T\}, \tag{12}$$

where $\text{sort}\{\cdot\}$ denotes the sorting function which returns the index vector of the elements of the input vector by sorting these elements in a descending order, and K is an integer parameter. Moreover, the g th element of the binary scrambling vector \mathbf{s} can also be generated by using the state z_q by

$$s_g = \text{abs}(\text{mod}(\text{int}(z_{K+g} \times 10^7), 2)), \tag{13}$$

where $\text{abs}(\cdot)$ denotes the operation to obtain the absolute value of the input, $\text{mod}(\cdot, 2)$ returns the remainder of an input divided by 2, and $\text{int}(\cdot)$ returns the integer part of the input which truncates the input at the decimal point. During the 2D chaotic encryption as described above, the initial values x_0, y_0, z_0 , and K can be set as the shared security keys between the transceiver. With numbers of about 16 decimal digits precision, the key space is more than 2^{172} , which is huge enough against eavesdropping using exhaustive attack methods [17].

2.3. PWC-Based mCAP

The schematic diagrams of the PWC encoding and decoding are illustrated in Figure 2a,b, respectively. Firstly, the quadrature amplitude modulation (QAM) constellation symbols corresponding to two paired subbands in an mCAP signal, i.e., subband 1 and subband 2, can be expressed by

$$x_{\text{SB1}} = a_n + jb_n, \tag{14}$$

$$x_{\text{SB2}} = c_n + jd_n, \tag{15}$$

where a_n and b_n are the I and Q parts of subband 1, and c_n and d_n are the I and Q parts of subband 2, respectively. In the encoding process, an angle rotation is firstly performed to obtain the following rotated constellation symbols:

$$x_{\text{SB1},\theta} = x_{\text{SB1}} e^{j\theta} = (a_n \cos \theta - b_n \sin \theta) + j(a_n \sin \theta + b_n \cos \theta), \tag{16}$$

$$x_{\text{SB2},\theta} = x_{\text{SB2}} e^{j\theta} = (c_n \cos \theta - d_n \sin \theta) + j(c_n \sin \theta + d_n \cos \theta), \tag{17}$$

where the rotation angle θ is usually set to $\theta = 45^\circ$ [15]. Then, the I and Q components of each rotated constellation symbols are interleaved. After interleaving, the transmitted signal of each subband can be obtained by

$$x_{\text{SB1,PWC}} = \text{Re}(x_{\text{SB1},\theta}) + j\text{Re}(x_{\text{SB2},\theta}) = (a_n \cos \theta - b_n \sin \theta) + j(c_n \cos \theta - d_n \sin \theta), \tag{18}$$

$$x_{\text{SB2,PWC}} = \text{Im}(x_{\text{SB1},\theta}) + j\text{Im}(x_{\text{SB2},\theta}) = (a_n \sin \theta + b_n \cos \theta) + j(c_n \sin \theta + d_n \cos \theta), \tag{19}$$

where $\text{Re}(\cdot)$ and $\text{Im}(\cdot)$ denote the operations to extract the I and Q parts of a complex-valued input, respectively.

In the decoding process, as shown in Figure 2b, the I and Q parts of the corresponding received signals $y_{\text{SB1,PWC}}$ and $y_{\text{SB2,PWC}}$ are firstly separated and then deinterleaving is executed correspondingly. Finally, an angle rotation is further performed to recover the transmitted QAM constellation symbols.

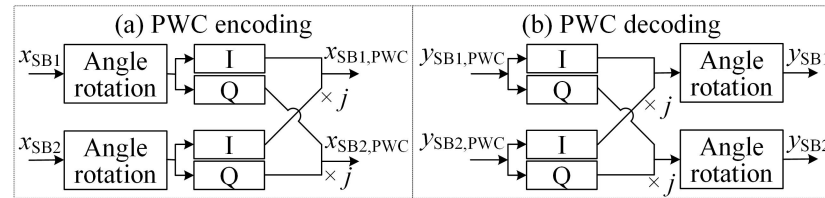


Figure 2. Schematic diagrams of (a) PWC encoding and (b) PWC decoding.

3. Results and Discussions

In this section, numerical simulations and hardware experiments are presented to investigate the performance of the proposed PWC-based m CAP-DM scheme with 2D chaotic encryption and compare it with other benchmark schemes. In our simulations and experiments, we considered the 4CAP case in which the overall bandwidth is divided into four subbands, i.e., $m = 4$. Moreover, each subblock was assumed to have two subbands, where one subband was selected to adopt constellation mode 1 while the remaining one adopted constellation mode 2 at each time slot, i.e., $N = 2$ and $k = 1$. The corresponding simulation parameters are shown in Table 2. To make a fair comparison, both 4CAP-DM and 4CAP-IM achieved the same SE of 2.5 bits/s/Hz. Specifically, the square 16-QAM constellation was used in 4CAP-IM, while the circular (7,1)-QAM constellation was adopted in 4CAP-DM. In our previous work [18], our simulation and experimental results showed that the circular (7,1)-QAM constellation achieved better BER performance than conventional square 8-QAM or 8-ary phase-shift keying (8-PSK) constellations in orthogonal frequency division multiplexing with dual-mode index modulation (OFDM-DM) based VLC systems. Therefore, the circular (7,1)-QAM constellation was adopted in 4CAP-DM in this work. Moreover, the interleaving-based constellation partitioning approach was considered to obtain two constellation modes from the circular (7,1)-QAM constellation. Please refer to our previous work [18] for more details. Since the basic 4CAP with general M -ary constellations cannot achieve a SE of 2.5 bits/s/Hz, it was not considered in our following simulations and experiments.

Table 2. Simulation Parameters.

Parameter	Value
Number of subbands (m)	4
Number of subbands in each subblock (N)	2
Number of activated subbands in each subblock (k)	1
Roll-off factor of RRCF	0.15
Upsampling factor	12
Spectral efficiency (SE)	2.5 bits/s/Hz
Simulation channel	AWGN

3.1. Simulation Results

Figure 3 shows the simulation BER versus SNR for 4CAP-IM and 4CAP-DM achieving the same SE of 2.5 bits/s/Hz over the additive white Gaussian noise (AWGN) channel. It can be clearly seen that 4CAP-DM requires a lower SNR to reach the 7% forward error correction (FEC) coding limit of $\text{BER} = 3.8 \times 10^{-3}$ in comparison to 4CAP-IM. More specifically, the

required SNRs for 4CAP-IM and 4CAP-DM to reach the BER threshold are 10.8 and 9.2 dB, respectively, indicating that 4CAP-DM outperforms 4CAP-IM by an SNR gain of 1.6 dB.

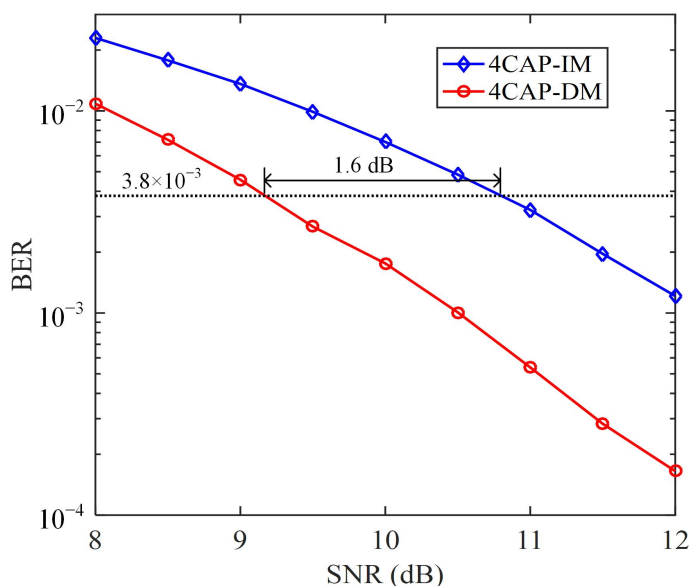


Figure 3. Simulation BER vs. SNR for 4CAP-IM and 4CAP-DM achieving the same SE of 2.5 bits/s/Hz over the AWGN channel.

3.2. Experimental Results

Based on the above simulation parameters, the corresponding hardware experiments were further performed. The experimental setup of a point-to-point VLC system using a blue mini-LED is illustrated in Figure 4, where the inset shows the photo of the overall experimental testbed. Firstly, the transmitted signal which was digitally generated offline by MATLAB was fed into an arbitrary waveform generator (AWG, Tektronix AFG31102) with a sampling rate of 250 MSa/s, where the signal bandwidth was set to 96 MHz. The AWG output signal was further combined with a 120 mA DC bias current via a bias-tee (MiniCircuits, ZFBT-6GW+) and the resultant signal was used to drive a blue mini-LED (HCCLS2021CHI03). Subsequently, a pair of biconvex lenses each with a diameter of 12.7 mm and a focal length of 20 mm were employed to ensure that most of the light emitted by the LED was focused on the active area of a photodetector (PD, Thorlabs PDA10A2). The PD had a bandwidth of 150 MHz and an active area of 0.8 mm². After that, the detected signal was recorded by a digital storage oscilloscope (DSO, LeCroy WaveSurfer432) with a sampling rate of 1 GSa/s, which was further processed offline by MATLAB. The detailed experimental parameters are given in Table 3.

Table 3. Experimental Parameters.

Parameter	Value
AWG sampling rate	250 MSa/s
Signal bandwidth	96 MHz
DC bias current	120 mA
Diameter of biconvex lenses	12.7 mm
Focal length of biconvex lenses	20 mm
Bandwidth of PD	150 MHz
Active area of PD	0.8 mm ²
DSO sampling rate	1 GSa/s

Figure 5a,b illustrate the measured nonlinear voltage–current curve and the low-pass frequency response of the system, respectively. It can be clearly observed that the system exhibits notable nonlinearity which is mainly caused by the blue mini-LED. We can also see

that the system reflects a typical low-pass characteristic which can result in an unbalanced SNR between the high-frequency subbands and the low-frequency subbands in the 4CAP signal.

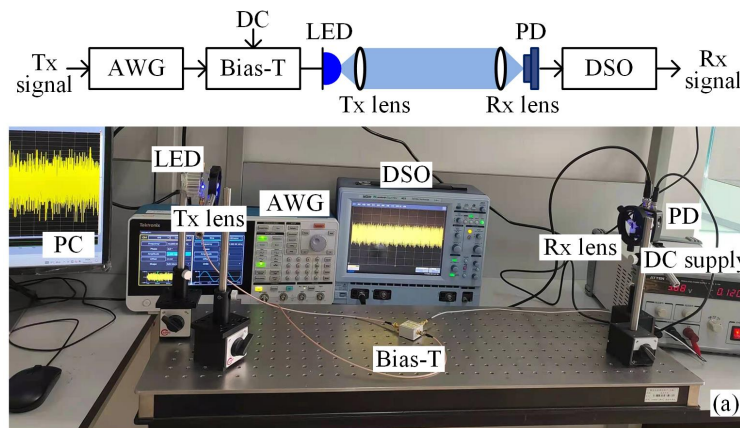


Figure 4. Experimental setup of a point-to-point VLC system using a blue mini-LED.

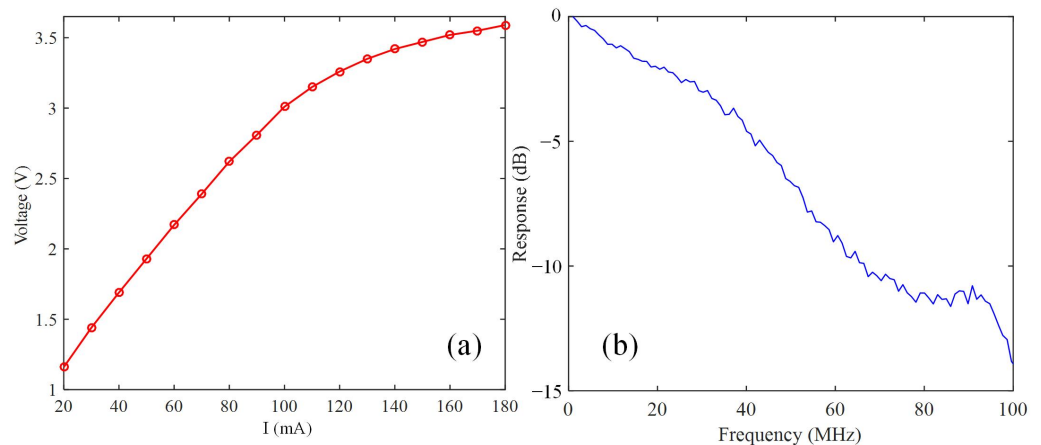


Figure 5. Measured (a) nonlinear voltage–current curve and (b) low-pass frequency response of the system.

Figure 6 shows the measured BER versus the peak-to-peak voltage (V_{pp}) of the AWG output signal for different cases, where the transmission distance is fixed at 80 cm. It can be clearly seen that 4CAP-DM greatly outperforms both 4CAP-IM and 4CAP-IM with PWC, achieving the lowest BER of 1.3×10^{-3} at $V_{pp} = 2$ V. Compared with 4CAP-DM, 4CAP-DM with PWC can achieve further significant BER improvement, obtaining the lowest BER of 4.45×10^{-4} at $V_{pp} = 2$ V. Moreover, nearly the same BER performance can be achieved for PWC-based 4CAP-DM with and without 2D chaotic encryption, suggesting that the application of 2D chaotic encryption does not affect the BER performance of PWC-based 4CAP-DM. It can also be observed that, for PWC-based 4CAP-DM with 2D chaotic encryption, the BER with no key and the BER with only the key for CMS are always about 0.38, and the BER with only the key for CCS is always about 0.21, which indicates that the application of 2D chaotic encryption can efficiently ensure the security of the transmitted 4CAP-DM signal. The insets (a)–(d) in Figure 6 depict the corresponding received constellation diagrams at $V_{pp} = 2$ V.

Figure 7 shows the measured BER versus the transmission distance for different cases with $V_{pp} = 2$ V. We can see that the BER of 4CAP-IM cannot reach the 7% FEC coding limit of $BER = 3.8 \times 10^{-3}$ when the distance is in the range from 80 to 110 cm. The maximum distances that can be transmitted by 4CAP-IM with PWC, 4CAP-DM, and 4CAP-DM with PWC at $BER = 3.8 \times 10^{-3}$ are 83.0, 87.0, and 98.8 cm, respectively. Hence, a 4.82% improvement of transmission distance can be achieved by 4CAP-DM in comparison to 4CAP-DM with PWC. Furthermore, distance extensions of 11.8 and 15.8 cm are obtained

by 4CAP-DM with PWC compared with 4CAP-IM with PWC and 4CAP-DM, which correspond to remarkable 13.56% and 19.04% improvements of transmission distance, respectively. It can also be seen that the PWC-based 4CAP-DM signal with 2D chaotic encryption cannot be successfully eavesdropped if the eavesdropper does not have the keys for both CCS and CMS at the same time.

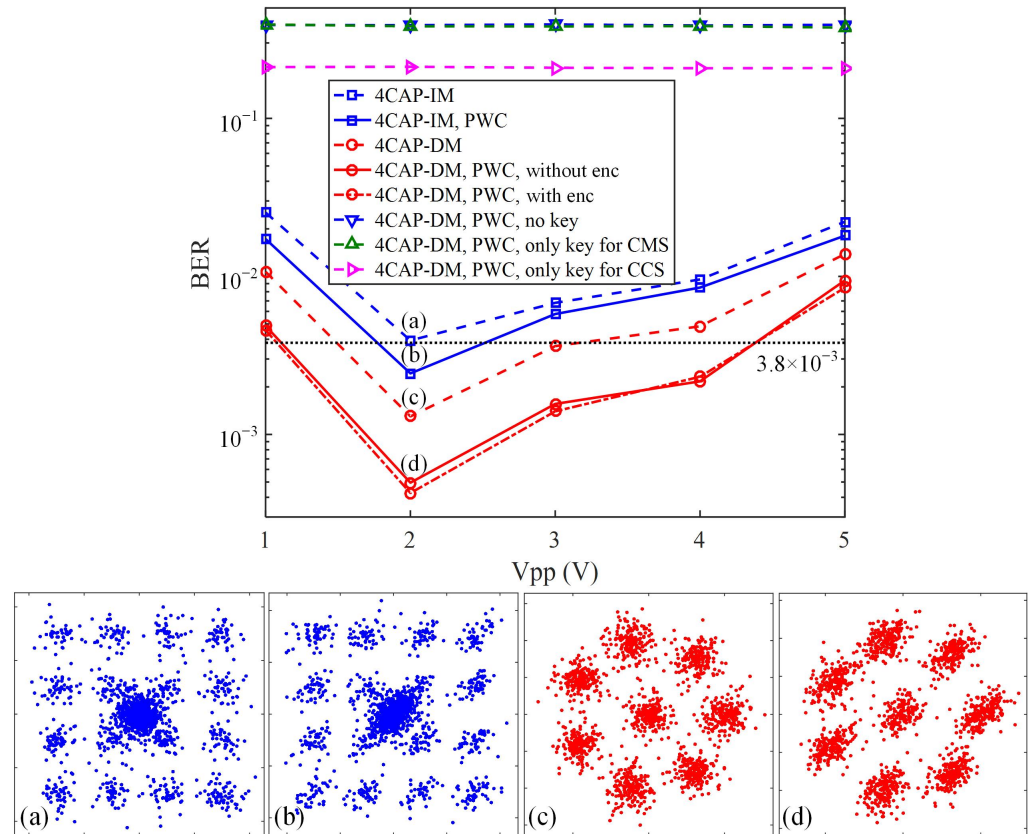


Figure 6. Measured BER vs. V_{pp} for different cases. Insets (a–d): the corresponding received constellation diagrams.

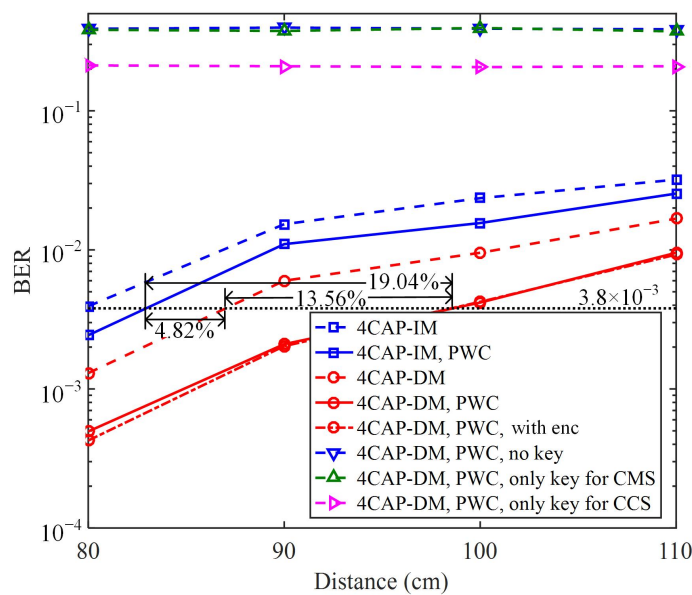


Figure 7. Measured BER vs. transmission distance for different cases.

4. Conclusions

In this paper, we proposed and evaluated a novel PWC-based *m*CAP-DM scheme with 2D chaotic encryption for secure, bandlimited VLC systems. The use of PWC coding can efficiently mitigate the SNR imbalance caused by the low-pass characteristic of LEDs, and the application of 2D chaotic encryption can successfully guarantee the security of the transmitted useful information in the VLC system. Simulation results validated the excellent BER performance of 4CAP-DM in comparison to 4CAP-IM, achieving the same SE of 2.5 bits/s/Hz over the AWGN channel. Furthermore, experimental results showed that PWC-based 4CAP-DM achieves much better BER performance than the benchmark schemes, while the physical-layer security of the system can be substantially enhanced by applying the 2D chaotic encryption approach. Therefore, the proposed PWC-based *m*CAP-DM scheme with 2D chaotic encryption can be a promising candidate for practical VLC systems.

Author Contributions: Conceptualization, C.C.; methodology, W.Z., Y.Y., X.D. and M.L.; validation, Y.Y.; formal analysis, W.Z. and X.D.; investigation, Y.N.; resources, Y.Y.; data curation, Y.N.; writing—original draft preparation, Y.N.; writing—review and editing, W.Z., X.D. and C.C.; supervision, M.L.; project administration, M.L.; funding acquisition, C.C. All authors have read and agreed to the published version of the manuscript.

Funding: This research was funded by the National Natural Science Foundation of China (61901065), the Natural Science Foundation of Chongqing (cstc2021jcyj-msxmX0480), and the Fundamental Research Funds for the Central Universities (2021CDJQY-013).

Institutional Review Board Statement: Not applicable.

Informed Consent Statement: Not applicable.

Data Availability Statement: Not applicable.

Acknowledgments: The authors would like to thank the anonymous reviewers for their valuable comments and suggestions.

Conflicts of Interest: The authors declare no conflict of interest.

References

1. Chi, N.; Zhou, Y.; Wei, Y.; Hu, F. Visible light communication in 6G: Advances, challenges, and prospects. *IEEE Veh. Technol. Mag.* **2020**, *15*, 93–102. [[CrossRef](#)]
2. Chen, C.; Fu, S.; Jian, X.; Liu, M.; Deng, X.; Ding, Z.G. NOMA for energy-efficient LiFi-enabled bidirectional IoT communication. *IEEE Trans. Commun.* **2021**, *69*, 1693–1706. [[CrossRef](#)]
3. Rajagopal, S.; Roberts, R.D.; Lim, S.K. Visible light communication: Modulation schemes and dimming support. *IEEE Commun. Mag.* **2012**, *3*, 72–82. [[CrossRef](#)]
4. Minh, H.L.; Brien, D.O.; Faulkner, G.; Zeng, L.; Lee, K.; Jung, D.; Oh, Y. High-speed visible light communications using multiple-resonant equalization. *IEEE Photonics Technol. Lett.* **2008**, *20*, 1243–1245. [[CrossRef](#)]
5. Chen, C.; Nie, Y.G.; Liu, M.; Du, Y.F.; Liu, R.S.; Wei, Z.X.; Fu, H.Y. Digital pre-equalization for OFDM-based VLC systems: Centralized or distributed? *IEEE Photonics Technol. Lett.* **2021**, *33*, 1081–1084. [[CrossRef](#)]
6. Wu, F.M.; Lin, C.T.; Wei, C.C.; Chen, C.W.; Huang, H.-T.; Ho, C.-H. 1.1-Gb/s White-LED-based visible light communication employing carrier-less amplitude and phase modulation. *IEEE Photonics Technol. Lett.* **2012**, *24*, 1730–1732. [[CrossRef](#)]
7. Chen, C.; Tang, Y.R.; Cai, Y.P.; Liu, M. Fairness-aware hybrid NOMA/OFDMA for bandlimited multi-user VLC systems. *Opt. Express* **2021**, *29*, 42265–42275. [[CrossRef](#)]
8. Elgala, H.; Mesleh, R.; Haas, H. Indoor broadcasting via white LEDs and OFDM. *IEEE Trans. Consum. Electron.* **2009**, *55*, 1127–1134. [[CrossRef](#)]
9. Chen, C.; Zhong, W.D.; Yang, H.L.; Du, P.F. On the performance of MIMO-NOMA based visible light communication systems. *IEEE Photonics Technol. Lett.* **2018**, *30*, 307–310. [[CrossRef](#)]
10. Haigh, P.A.; Le, S.T.; Zvanovec, S.; Ghassemlooy, Z.; Luo, P.; Xu, T.; Chvojka, P.; Kanesan, T.; Giacomidis, E.; Canyelles-Pericas, P.; et al. Multi-band carrier-less amplitude and phase modulation for bandlimited visible light communications systems. *IEEE Wirel. Commun.* **2015**, *22*, 46–53. [[CrossRef](#)]
11. Akande, K.O.; Popoola, W.O. Subband index carrierless amplitude and phase modulation for optical communications. *J. Lightwave Technol.* **2018**, *36*, 4190–4197. [[CrossRef](#)]

12. Wang, Z.; Zhang, J.W.; He, Z.X.; Zou, P.; Chi, N. Subcarrier index modulation super-Nyquist carrierless amplitude phase modulation for visible light communication systems. *J. Lightwave Technol.* **2021**, *39*, 6420–6433. [[CrossRef](#)]
13. Hu, W.X.; Zhang, M.; Li, Z.; Popov, S.; Leeson, M.S.; Xu, T. High-dimensional feature based non-coherent detection for multi-intensity modulated ultraviolet communications. *J. Lightwave Technol.* **2021**. [[CrossRef](#)]
14. Zuo, T.; Wang, F.S.; Zhang, J.K. Sparsity signal detection for indoor GSSK-VLC system. *IEEE Trans. Veh. Technol.* **2021**, *70*, 12975–12984. [[CrossRef](#)]
15. He, J.; He, J.; Shi, J. An enhanced adaptive scheme with pairwise coding for OFDM-VLC system. *IEEE Photonics Technol. Lett* **2018**, *30*, 1254–1257. [[CrossRef](#)]
16. Yang, Y.B.; Chen, C.; Zhang, W.; Deng, X.; Du, P.F.; Yang, H.L.; Zhong, W.D.; Chen, L.Y. Secure and private NOMA VLC using OFDM with two-level chaotic encryption. *Opt. Express* **2018**, *26*, 34031–34042. [[CrossRef](#)] [[PubMed](#)]
17. Kordov, K.; Stoyanov, B. Least significant bit steganography using Hitzl-Zele chaotic map. *Int. J. Electron. Telecommun.* **2017**, *63*, 417–422. [[CrossRef](#)]
18. Chen, C.; Nie, Y.G.; Ahmed, F.; Zeng, Z.H.; Liu, M. On the Constellation Design of DFT-S-OFDM with Dual-Mode Index Modulation in VLC. 2022. Available online: https://www.researchgate.net/publication/357747021_On_the_constellation_design_of_DFT-S-OFDM_with_dual-mode_index_modulation_in_VLC (accessed on 11 February 2022).